New Journal of Physics
The open-access journal for physics

STM studies of the self-assembly of manganese porphyrin catalysts at the Au(111)—*n*-tetradecane interface

Bas Hulsken[1], Johannes A A W Elemans[1,3], Jan W Gerritsen[1], Tony Khoury[2], Maxwell J Crossley[2], Alan E Rowan[1], Roeland J M Nolte[1] and Sylvia Speller[1]

[1] Institute for Molecules and Materials, Radboud University Nijmegen, Toernooiveld, 6525 ED Nijmegen, The Netherlands
[2] School of Chemistry, University of Sydney, NSW 2006, Australia
E-mail: J.Elemans@science.ru.nl

New Journal of Physics **11** (2009) 083011 (14pp)
Received 6 January 2009
Published 12 August 2009
Online at http://www.njp.org/
doi:10.1088/1367-2630/11/8/083011

Abstract. The precise structure of monolayers of catalytic manganese porphyrins at the interface of an Au(111)-surface and an *n*-tetradecane liquid has been determined in a liquid-cell scanning tunneling microscope (STM). Before the addition of the manganese porphyrins, an ordered monolayer of lamellae of *n*-tetradecane molecules on the Au(111) surface could be imaged. It was found that only domain boundaries in this monolayer were correlated to the underlying gold surface, but not the orientation of the *n*-tetradecane lamellae and the molecules within them. Both the reconstruction of the Au(111) surface and the ordering of the first layer of *n*-tetradecane can direct the ordering of the manganese porphyrins that are subsequently added to the liquid phase.

[3] Author to whom any correspondence should be addressed.

Contents

1. Introduction **2**
2. Experimental **3**
2.1. STM setup . . . 3
2.2. Preparation of the Au(111) surface . . . 3
2.3. Preparation of the *n*-tetradecane liquid . . . 3
2.4. STM topography measurements . . . 4
2.5. Correlation methods . . . 4
3. Results and discussion **6**
3.1. Structure of the Au(111)/*n*-tetradecane interface . . . 6
3.2. Self-assembly of manganese porphyrins at the Au(111)−*n*-tetradecane interface 9
4. Conclusions **13**
Acknowledgments **13**
References **13**

1. Introduction

While many conventional spectroscopic techniques are available to study reaction mechanisms at the ensemble level, it is only recently that fluorescence microscopy has been applied to monitor, by single turnover counting, chemical reactions carried out on crystal faces [1] and by enzymes [2]. With the advent of scanning probe microscopy, it has become possible to image chemical reactions even down to the atomic level, albeit under idealized conditions [3]. During the past few years, we have developed a highly sophisticated STM setup equipped with an inert liquid cell and a bell jar that can be filled with any gas desired. Using this equipment, surfaces can be studied at solid–liquid interfaces under very clean conditions, comparable to those in ultrahigh vacuum (UHV) [4]. Currently, one of the most appealing challenges of scanning probe research is to go beyond just the imaging of molecules, and to study dynamic processes that occur at the chemically highly relevant environment of a solid–liquid interface [5]. In particular, studying chemical reactions at such an interface is highly interesting, since it resembles the environment in which most chemical reactions in academic and industrial laboratories take place. In a liquid-cell STM, we have very recently succeeded for the first time to image at a solid–liquid interface a multi-step catalytic oxidation reaction at the single catalyst level [6]. Manganese(III) porphyrin catalysts Mn1 (figure 1) were immobilized flat at the interface of an Au(111) surface and an *n*-tetradecane solution, and the resulting catalytic monolayer appeared highly active in oxidizing alkene molecules, which were added to the liquid phase, into epoxides. During the course of the catalytic studies, we became aware of the essential role that the solid–liquid interface seems to play with respect to the ordering and the catalytic performance of the porphyrin monolayer. For example, we suspected a prominent role of the gold surface in binding to the manganese metal in the center of the porphyrins, because under the same conditions porphyrins that do not contain a metal center were found not to adsorb to the same solid–liquid interface [7]. For this reason it was our aim to investigate in high detail the nature of the interface between Au(111) and *n*-tetradecane, and the subsequent

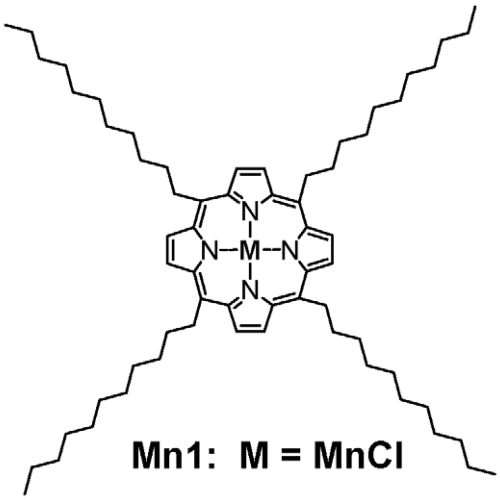

Figure 1. Molecular structure of manganese porphyrin catalyst Mn1.

adsorption of Mn1 porphyrins to this interface. Here we report detailed STM studies of these investigations, which will demonstrate that a monolayer of adsorbed *n*-tetradecane molecules can influence the subsequent ordering of the porphyrins, and that this ordering is also influenced by the reconstruction present on the Au(111) surface.

2. Experimental

2.1. STM setup

The liquid-cell STM setup was home-built based on earlier designs [4, 8]. The liquid cell was made of an inert polymer (Kel-F) and the electrode for the sample bias voltage of platinum. The sample holder was made out of gilded steel, and held in place by a magnet outside of the liquid cell. The entire STM was placed under a bell jar, which can be flushed with argon or oxygen.

2.2. Preparation of the Au(111) surface

Au(111) surfaces were prepared by evaporating 99.99% gold on freshly cleaved mica. The gold was grown epitaxially on the heated mica ($< 300\,^{\circ}$C), at a pressure of 10^{-7} mbar, and annealed for 2 h at 300 °C at a pressure of 10^{-8} mbar. It was found that the quality of the gold films deteriorated quickly, and therefore gold films no older than 2 days were used in the present study. Just before mounting the film in the liquid cell it was annealed in a hydrogen flame.

2.3. Preparation of the n-tetradecane liquid

n-Tetradecane was purchased from Aldrich and twice distilled under reduced pressure before use. It was purged extensively (>12 h) with argon prior to the STM experiment to ensure the removal of any other gases dissolved in the liquid.

2.4. STM topography measurements

STM measurements were performed in a home-built liquid-cell STM connected to an Omicron SCALA SPM controller. STM tips were mechanically cut from platinum–iridium (80–20) wire. All STM images presented are constant current images, typically applying a very low tunneling current of around 10 pA, and have been corrected for background slope (by subtracting a plane). In all cases, the bias voltage was applied to the Au(111) surface. Some spike noise was removed by filtering the data through a median filter with a [3 × 3] pixel filter size (only the STM images in figure 2).

2.5. Correlation methods

A crystalline surface is an endless repetition of one unique unit cell; one can reason that an STM image of an n unit cell large area of a crystalline surface is equivalent to n STM images of a 1 unit cell large area. In this paper, the positions of the individual unit cells were determined by performing a correlation between a manually selected part of the STM image, which contains at least one unit cell, and the complete STM image [9]. The correlation averaging procedure will be explained here by a relatively simple model system, i.e. a monolayer of non-symmetric organic molecules on a graphite surface (figures 2(A) and (B)). First, a small reference area, containing at least one unit cell, is selected manually in an STM image of the monolayer (figure 2(C)). The filter program then searches, by means of correlation, the entire STM image for areas equivalent to the selected reference area. Subsequently, the found areas are sorted by their degree of similarity to the reference area, which is quantified by the correlation coefficient. Which of the found areas are similar enough to the reference area to be used for the correlation averaging procedure can usually be readily established by identifying the correlation maxima and the distribution of the equivalent areas found over the STM image in an intermediate correlation map (figure 2(E)). This identification, which is the second interactive step in the correlation averaging procedure, allows for the localization and subsequent extraction of n different STM sub-images, which are situated at a grid with the same spacing as the unit cells. This division in sub-images is used for two things: firstly, by averaging the n different sub-images, an STM image with the size of the sub-image is obtained with a sqrt(n) reduction in noise (cf figure 2(D)); and secondly, because the positions of the unit cells in the original STM image, as found by the correlation method, represent the crystal lattice, an accurate measurement of the unit cell's dimensions can be obtained. For the noise reduction, the sub-images used for the averaging are replaced by the averaged sub-image in the original STM image (figure 2(F)).

In addition to a reduction in noise and enhanced resolution, the correlation method offers another important use: it can provide quantitative information about the errors in the measurement of distances and angles in an STM image. The correlation filter finds the spatial positions of areas in the STM image that are equivalent to the selected reference area. If the STM image would be a map of a perfect 2D crystalline lattice on a surface, then the spatial distribution of these equivalent areas would exactly match this crystalline lattice. However, for many STM images this equivalency is not the case. If the correlation filter is applied using areas that are wrongly marked as equivalent, then the filter results in a distorted image and the quantitative data about angles and distances are wrong. It is therefore essential that

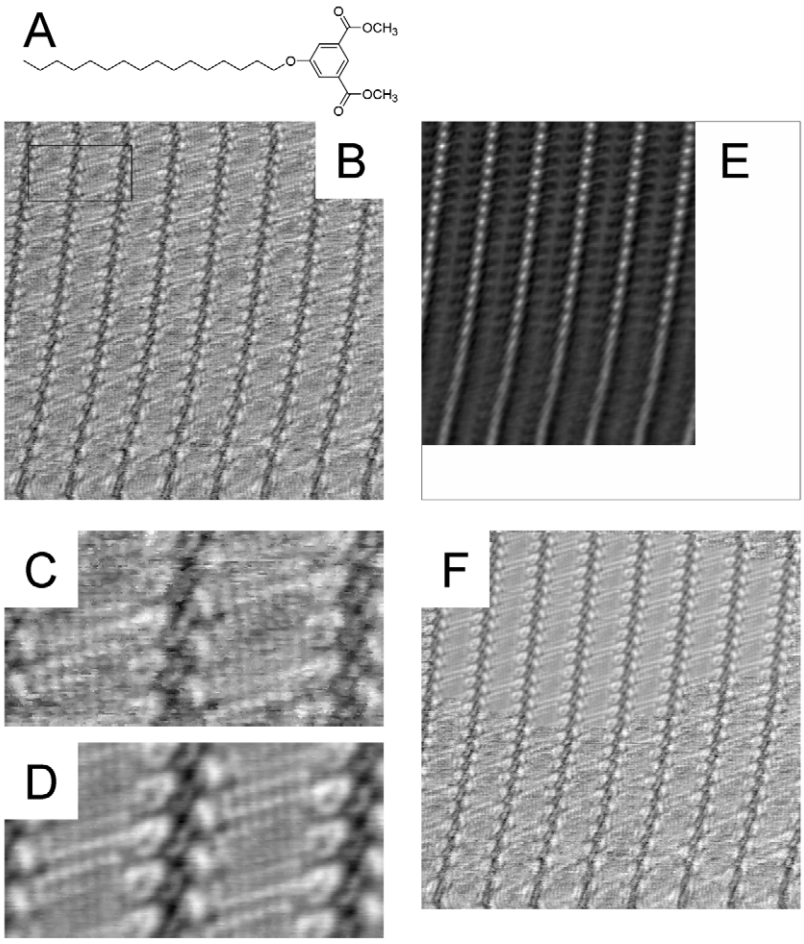

Figure 2. Outline of the correlation averaging method used in this paper. (A) Molecular structure of 5-hexadecyloxy-isophthalic acid dimethyl ester, the molecule used for explaining the procedure. (B) STM image (15×15 nm) of a self-assembled monolayer of this molecule at the interface of graphite and 1-phenyloctane; the black rectangle in the top left corner represents the selected sub-image to be used for correlation averaging. (C) Original sub-image (rectangle in (B)). (D) Averaged sub-image for n positions with highest correlation. (E) Intermediate correlation map of the STM image obtained by using the selected sub-image; note that in the top left corner the correlation maxima, as expected, are most pronounced. (F) Correlation averaged STM image that is obtained by substitution of the averaged sub-image in the original STM image.

the selection of the equivalent areas is an interactive step, during which an experienced user can judge whether areas are truly equivalent, or merely similar. In fact, the filtering software is a powerful tool to identify irregularities in otherwise periodical structures, such as different domains in monolayers of adsorbed molecules, and steps or defects in a crystal lattice.

3. Results and discussion

3.1. Structure of the Au(111)/n-tetradecane interface

First, the interface between Au(111) and *n*-tetradecane was studied with STM. At the interface with a flat gold surface, liquids of *n*-alkanes are known to have a layered ordering with the main axis of their molecules oriented parallel to the surface [10]. At the *n*-hexadecane–Au(001) interface, for example, three to four of such layers are present (at 350 K), with the first layer at a position 3–4 Å above the top layer of gold atoms (center-to-center distance). At the interface of *n*-tetradecane with a Au(111) surface, the liquid forms a crystalline monolayer above the bulk melting temperature of 5.9 °C, which is high enough to have areas of the interface covered by a uniform crystalline monolayer even at room temperature. Our experiments show that, similar to that observed for a Au(111) surface exposed to UHV, Au(111) submerged in *n*-tetradecane has a reconstructed surface, which can be seen as the lighter double zigzag lines in the STM images in figure 3. The herringbone pattern of this reconstruction can be used as a ruler to calibrate the STM images, which allows for a highly accurate measurement of distances and angles.

It can be seen that the Au(111)–*n*-tetradecane interface, which has been measured in the controlled environment of the liquid-cell STM, is well-defined and relatively free of defects. The *n*-tetradecane molecules are organized in extended lamellae, in which the long axes of the molecules make a 60° angle with the interlamellar grooves. A close-up of individual *n*-tetradecane molecules in the monolayer is shown in figure 3(C); underneath them, the $23 \times \sqrt{3}$ reconstruction of the gold is still present and visible. A cross-section taken perpendicularly through two periods of the reconstruction is shown in figure 3(D). The observed period, shape and corrugation of this reconstruction are in agreement with values that have been previously obtained by UHV-STM measurements [11]. The potential presence of ordered layers of *n*-tetradecane above the first adsorbed monolayer of *n*-tetradecane [12] will reduce the diffusion constant perpendicular to the surface, which might be one of the causes for the very low amount of contaminations observed at the interface. However, evidence for the actual existence of these layers under the experimental conditions used could not be established by STM measurements.

In order to determine the precise orientation of the individual *n*-tetradecane molecules with respect to the lamellar structure and the underlying Au(111) surface, the unit cell of the *n*-tetradecane monolayer was analyzed using the correlation method. The analysis was performed on the STM measurement shown in figure 3(A), on both the domains A and B. The distributions of measured angles and lengths of the longest unit cell vector of the *n*-tetradecane monolayer in domain A in figure 3(A) are shown in figure 4.

Table 1 shows that within the monolayer the *n*-tetradecane molecules are packed quite tightly along the long axis (t_l), with an *n*-tetradecane molecule being 18.5 Å long. Along the short axis (t_s) the packing is less tight. The width of an *n*-tetradecane molecule is 3.1 Å in-plane with the carbon–carbon bonds and 2.2 Å perpendicular to that plane, which suggests that the molecules are oriented with their carbon–carbon bonds parallel to the Au(111) surface, as illustrated in figure 3(C). The orientation of the lamellae, the domain boundaries in the monolayer and the width of the lamellae were measured manually from the STM images. From the calibrated STM images in figure 3 and the corresponding data, which are collected in table 2, it can be concluded that only the direction of the domain boundaries (along the $[1\bar{1}0]$-direction) and the orientation of the *n*-tetradecane molecules in the lamellae (60° tilt with respect to the lamellar groove) are well defined. The orientation of the lamellae with respect

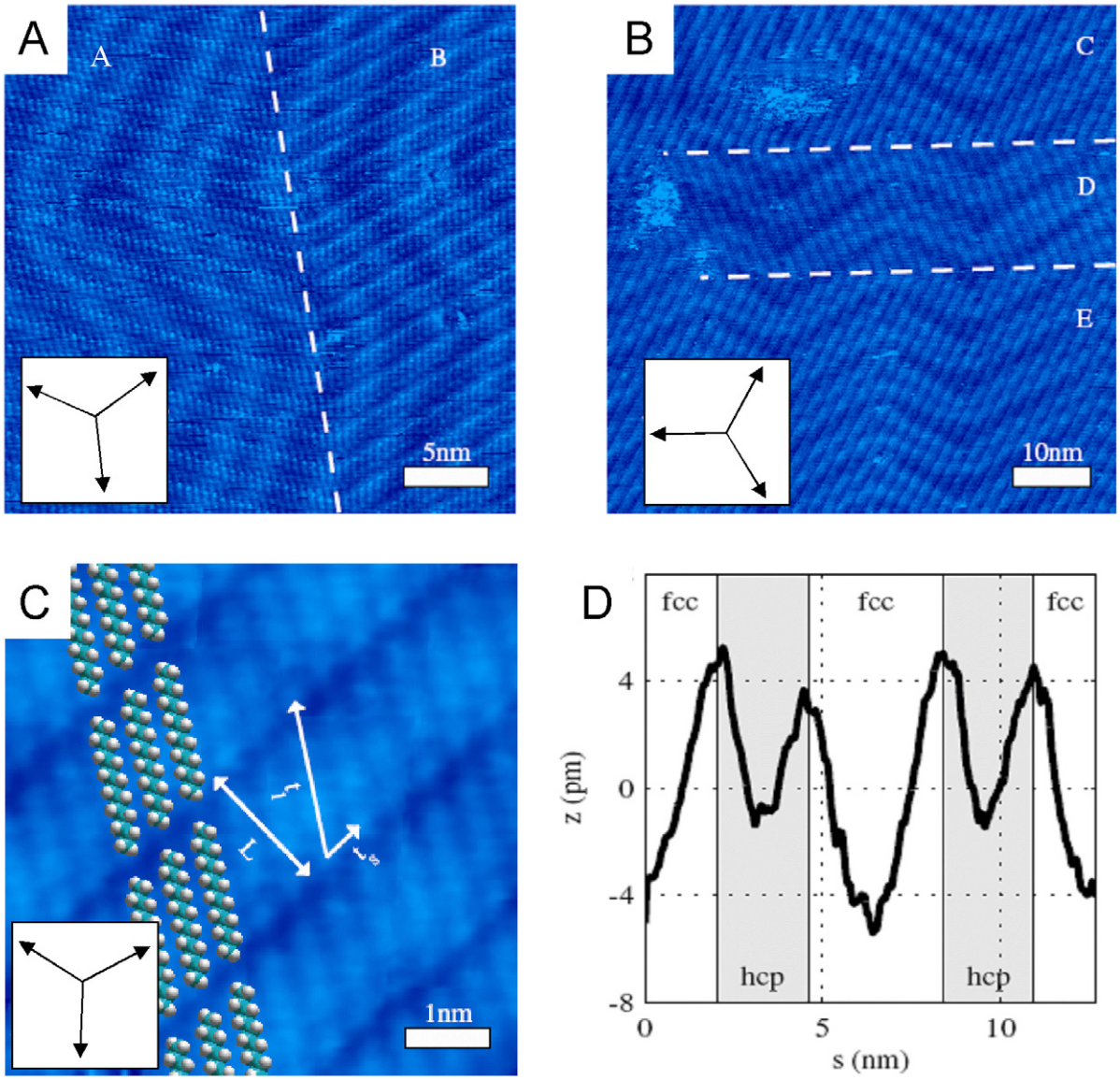

Figure 3. (A)–(C) Calibrated constant current STM images of the interface between an Au(111) surface and an *n*-tetradecane liquid; the dashed lines indicate domain boundaries and the vectors in the bottom left corner indicate main $[1\bar{1}0]$ crystal directions of the gold lattice. (A) $I = 15\,\text{pA}$, $V_{\text{sample}} = 200\,\text{mV}$. (B) $I = 5\,\text{pA}$, $V_{\text{sample}} = 200\,\text{mV}$. (C) $I = 10\,\text{pA}$, $V_{\text{sample}} = 300\,\text{mV}$. The image was correlation averaged to make the individual molecules more clear. Both the reconstruction of the gold surface and the individual $C_{14}H_{30}$ molecules are discernible, and several molecular models are drawn in to indicate the structure of the monolayer. (D) Cross-section along one of the $[1\bar{1}0]$ directions in (A) through the two periods of the reconstruction, which shows the typical reconstruction period and the alternating fcc/hcp domains.

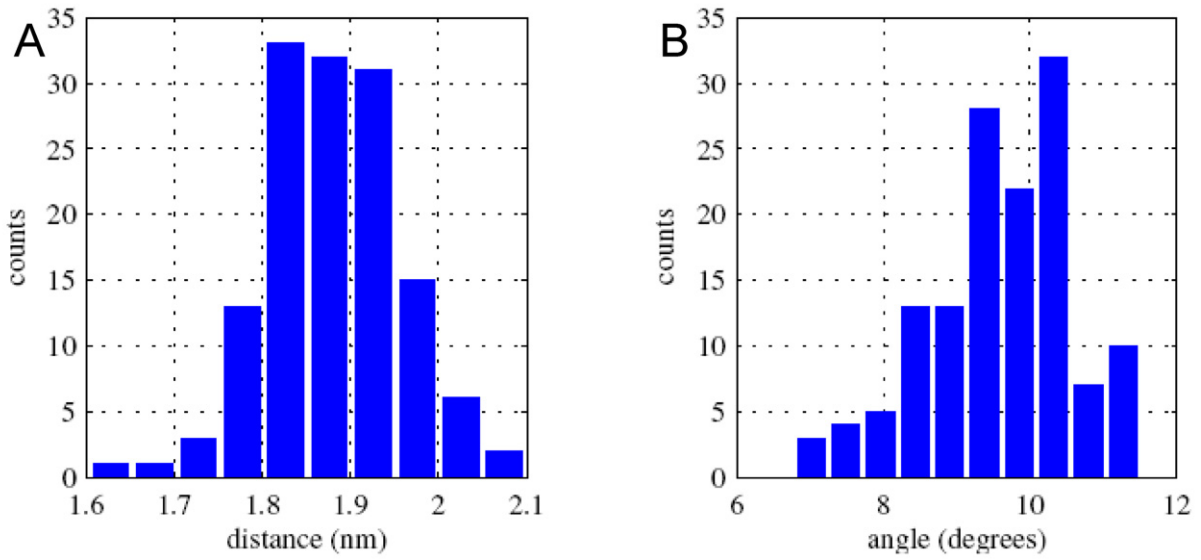

Figure 4. (A) Distribution of measured lengths of the unit cell vector along the long axis of the *n*-tetradecane molecules in domain A of the monolayer shown in figure 3(A), determined by correlation. The mean value is 1.88 nm with a standard deviation of 0.08 nm. (B) Distribution of measured angles between the unit cell vector along the long axis of the *n*-tetradecane molecules and the nearest $\langle 1\bar{1}0\rangle$-direction. The mean value is 10° with a standard deviation of 1°.

to the underlying gold lattice, and therefore also the orientation of the individual molecules within the lamellae to that surface, varies significantly over different STM measurements. This variation is most evidently observed by the angle between the lamellae on either side of a domain boundary: this angle is always significantly larger than 120°, which makes it impossible for both domains to have lamellae oriented along equivalent crystal directions. These observations are in contradiction with previous experiments in the literature, which reported that the long axis of the *n*-tetradecane molecules is always oriented parallel to one of the main $\langle 1\bar{1}0\rangle$ directions of the gold lattice [13]. Molecular dynamics studies have shown that domains with intermolecular alignment can form on any border of an *n*-alkane liquid, because the interaction between long chain *n*-alkane molecules is strong enough to form ordered domains [10]. The STM measurements shown here corroborate the finding that the crystal structure of the Au(111) surface at the interface does not have a large influence on the molecular orientation of the *n*-tetradecane molecules in the adsorbed monolayer. Our observation that the domain boundaries in the monolayer are fixed with respect to the Au(111) crystal structure is remarkable, but not straightforward to explain. A careful analysis of the STM images in figure 3 reveals that typically at the domain boundaries themselves the *n*-tetradecyl chains seem to be immobilized in an orientation parallel to one of the main $\langle 1\bar{1}0\rangle$ directions. This indicates that a significant interaction exists between these molecules and the underlying gold lattice, which might be related to local commensurability. The fact that further away from the domain boundaries the *n*-tetradecane chains do not follow the directions of the gold anymore, might be attributed to strong intermolecular interactions within the tightly packed lamellae, which dictate the ordering of the molecules and weaken possible interactions with the underlying gold. On top of or close to

Table 1. Orientation of the molecules of *n*-tetradecane on Au(111) in domains A, B and D in figure 3, as determined by the correlation method, where $\vec{t}_l$ is the long unit cell vector of the *n*-tetradecane monolayer, the long axis of the molecule is along this vector and $\vec{t}_s$ is the short unit cell vector. *L* denotes the width of the lamellae, which has been calculated by taking the inner product of $\vec{t}_l$ and $\vec{t}_s$ (see figure 3). The errors given represent the standard deviations of the measurements.

Domain	$\angle(\vec{t}_l, \langle 1\bar{1}0\rangle)$ (±2°)	$\angle(\vec{t}_s, \langle 1\bar{1}0\rangle)$ (±3°)	$\angle(\vec{t}_l, \vec{t}_s)$ (±3°)	$\lvert\vec{t}_l\rvert$ (±0.5 Å)	$\lvert\vec{t}_s\rvert$ (±0.1 Å)	*L* (±0.6 Å)
A	9°	8°	59°	19.1 Å	5.5 Å	16.4 Å
B	−6°	−6°	60°	18.9 Å	5.4 Å	16.4 Å
D	−4°	−6°	62°	19.7 Å	5.1 Å	17.4 Å

Table 2. Orientation of the lamellae of *n*-tetradecane on Au(111) in various domains (see figure 3), where $\vec{d}$ denotes the orientation of the domain boundary, $\vec{l}$ the orientation of a lamella, and $\vec{l}_1$, $\vec{l}_2$ the orientation of the long axis of the *n*-tetradecane molecules. *L* represents the lamellar distance. The errors given represent the standard deviations of the measurements.

Orientation (domain)	$\angle(\vec{d}, \langle 1\bar{1}0\rangle)$ (±2°)	$\angle(\vec{l}, \langle 1\bar{1}0\rangle)$ (±2°)	$\angle(\vec{l}_1, \vec{l}_2)$ (±2°)	*L* (±0.5 Å)
a (A, B)	2°	8, −8°	136°	16.4, 16.2 Å
b (C, D, E)	2, 2°	4, −7, 2°	132, 129°	16.9, 17.5, 16.3 Å
c	2°	10, −5°	135°	17.6, 17.5 Å
d	2, 2°	2, −5°	128°	16.9, 17.4 Å

the domain boundary, these intermolecular interactions become weaker due to the decreasingly tight intermolecular packing, and molecule–substrate interactions start to play a more dominant role.

3.2. Self-assembly of manganese porphyrins at the Au(111)−n-tetradecane interface

Now that the solid–liquid interface between Au(111) and *n*-tetradecane has been well-characterized and calibrated, the adsorption of manganese porphyrin Mn1 at this interface will be investigated. A dilute solution ($\sim 10^{-5}$ M) of Mn1 was prepared in distilled and argon-purged *n*-tetradecane. The liquid-cell STM was filled with this solution and a flame-annealed Au(111) film was mounted in the liquid cell immediately after annealing. After flushing the bell jar with argon, the STM measurement was started. In the first STM image taken, approximately 15 min after submerging the Au(111) surface in the solution, a fully formed self-assembled monolayer of Mn1 was observed at the solid–liquid interface (figure 5). Note that STM is temporally slow and might not be sufficiently quick to detect a dynamic rearrangement upon the adsorption of the porphyrins. In the STM image, the herringbone pattern of the Au(111) $23 \times \sqrt{3}$ reconstruction is still clearly visible as bright wide bands modulating the finer structure of the porphyrin monolayer. The appearance of the reconstruction is similar to that observed for clean Au(111).

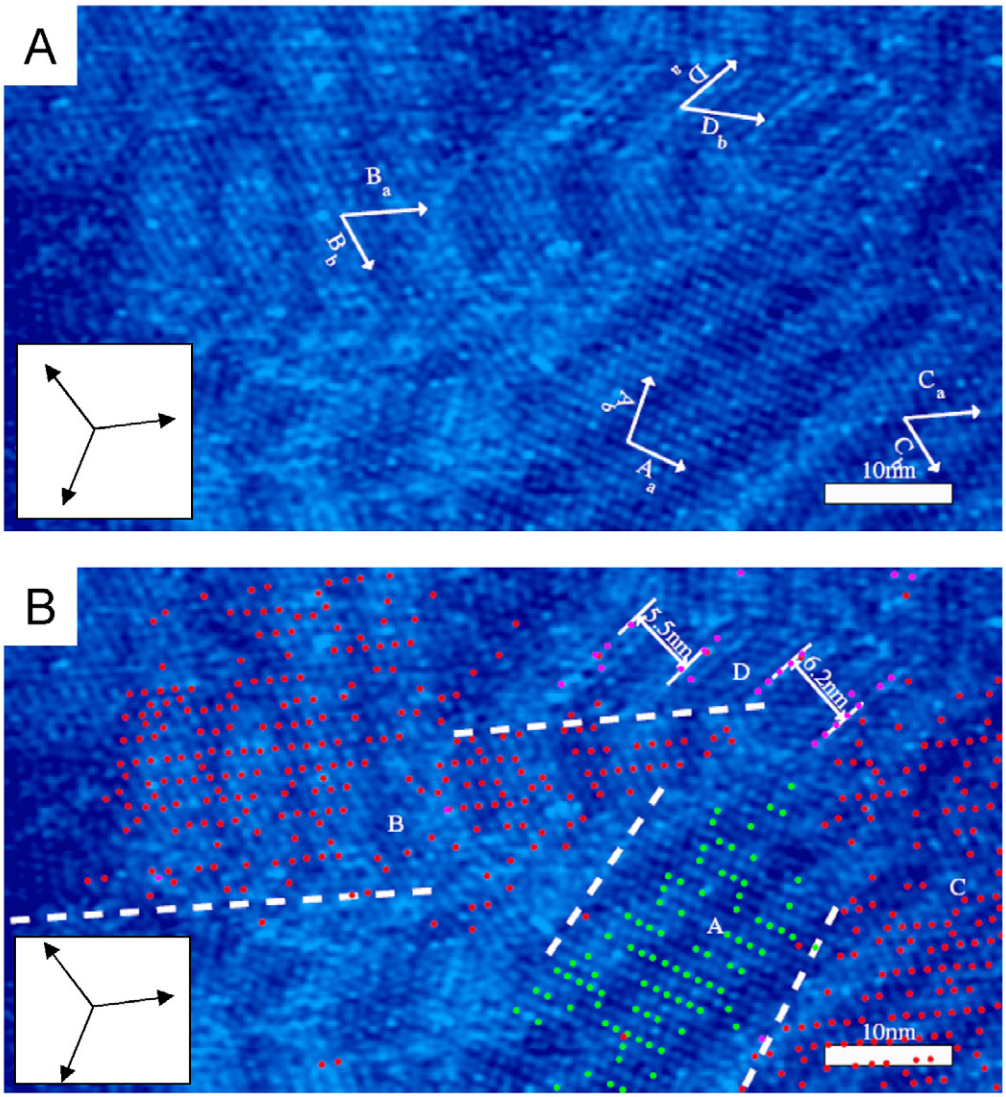

Figure 5. (A) Calibrated constant current STM image ($I = 5\,\text{pA}$, $V_{\text{sample}} = -200\,\text{mV}$) of a self-assembled monolayer of Mn1 at the Au(111)−*n*-tetradecane interface. The Au(111) reconstruction, which is visible through the finer structure of the porphyrin monolayer as bright wide bands, has been used to calibrate the image. Four large domains A–D are distinguishable in the monolayer and their respective lattice vectors have been drawn in each domain as a visual guide to the eye. The vectors in the bottom left corner indicate main $[1\bar{1}0]$ crystal directions of the gold lattice. (B) The same STM image, but with the unit cells found by the correlation method drawn in. Unit cells in domain A are marked by green dots, unit cells in the identical domains B and C by red dots, and unit cells in domain D by magenta dots. The white dashed lines are a best attempt of marking the domain boundaries; their position and orientation should be considered to have relatively large errors (±5 nm, ±5°).

Table 3. Lattice parameters of the unit cells of the various domains of the monolayer of Mn1 at the Au(111)–*n*-tetradecane interface. For domains A, B, C (see figure 5), E and F (figure 6) the lattice vectors have been determined by the correlation method. Domain D (figure 5) is too small and too poorly resolved to apply the correlation method; in this case, the values have been measured manually. For domains A, B and C, $\vec{b}$ is the longest lattice vector, spanning two porphyrins, and $\vec{a}$ is the shortest lattice factor, spanning one porphyrin. For domains D, E and F, the unit cells consist of only one porphyrin molecule. L is the height of the unit cell containing two porphyrins (domains A, B and C), which has been determined by the component of $\vec{b}$ perpendicular to $\vec{a}$. The errors given represent the standard deviations of the measurements.

Domain	$\angle(\vec{a}, \langle 1\bar{1}0\rangle)$ ($\pm 2°$)	$\angle(\vec{b}, \langle 1\bar{1}0\rangle)$ (± 2)	$\angle(\vec{a}, \vec{b})$ ($\pm 2°$)	$\lvert\vec{a}\rvert$ (± 0.5 Å)	$\lvert\vec{b}\rvert$ (± 0.5 Å)	L (± 1 Å)
A	27°	4°	83°	9.9 Å	21.2 Å	21 Å
B = C	−1°	−7°	66°	12.0 Å	19.6 Å	18 Å
D	$34 \pm 4°$	$-16 \pm 4°$	$49 \pm 4°$	11.3 ± 1 Å	7.9 ± 1 Å	
E	31°	−12°	78°	10.1 Å	14.4 Å	
F	−31°	9°	81°	10.6 Å	13.8 Å	

Interestingly, as is the case for the adsorption of *n*-tetradecane, the adsorption of Mn1 does not seem to affect this reconstruction to an appreciable extent.

In the STM image in figure 5(A), four domains with a different porphyrin ordering are observed. In order to determine their unit cells, the correlation method was applied, which revealed that the porphyrins in domains B and C have the same lattice, in spite of the fact that the reconstructed Au(111) surface in domain B has a different orientation from that in domain C. This observation indicates that the surface reconstruction does not uniquely determine the orientation of the molecules of Mn1 in the monolayer. Because the porphyrins in domain D are less well resolved than those in the other domains, its lattice vectors can only be determined with a larger error. Figure 5(B) shows the unit cells in the various domains of the monolayer that were found by the correlation method. The domain boundaries are difficult to discern, because the monolayer is less organized around them. The dashed lines are a best effort indication of these domain boundaries, but their exact positions and orientations will have a relatively large uncertainty.

From the distribution of the unit cells in domains A, B and C, an observation can be made that cannot be easily seen by the naked eye in figure 5(A): the porphyrin monolayer has a superstructure. Each of the unit cells in these domains, as found by the correlation method, contains not one, but two porphyrin molecules. For domain D, the correlation method finds an even larger unit cell. The measured parameters of the lattices are summarized in table 3.

Clearly, in domain D, the short lattice vector $\vec{D}_a$ runs along the herringbone lines of the Au(111) reconstruction. Considering the length of the long lattice vector $\vec{D}_b$, it is most likely determined by the length of the unit cell of the Au(111) reconstruction, which is 63 ± 0.5 Å [13]. However, the measured width L of the unit cell of the superstructure in domain D is 5.3 nm, which is significantly smaller. This difference probably indicates that the superstructure is the result of a superposition of the porphyrin lattice and the herringbone of the surface

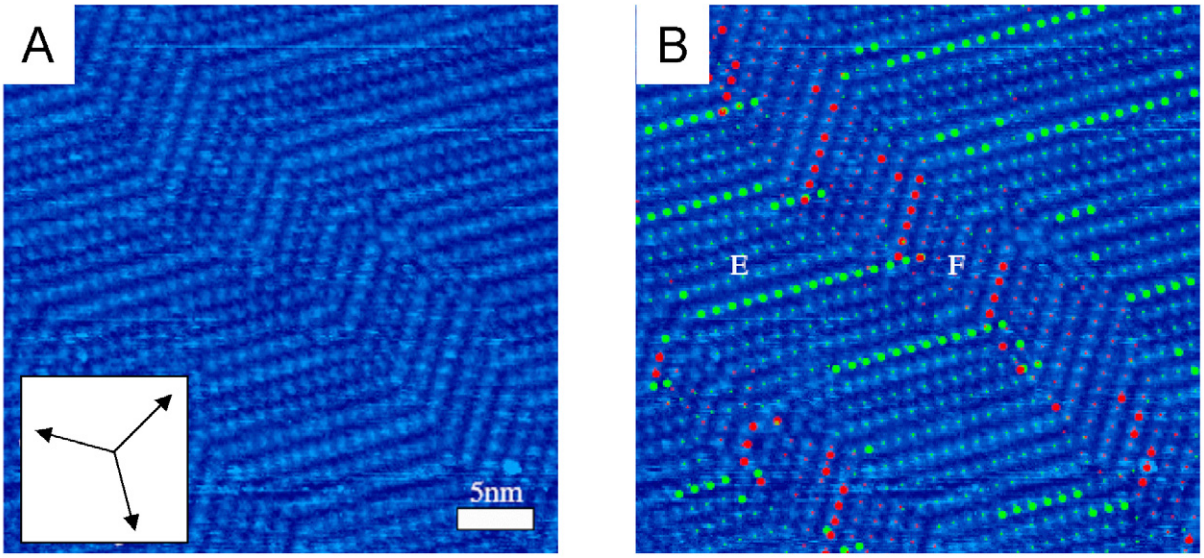

Figure 6. Calibrated constant current STM image ($I = 3$ pA, $V_{\text{sample}} = -200$ mV) of a self-assembled monolayer of Mn1, in which a superstructure is clearly present, at the Au(111)−*n*-tetradecane interface. The vectors in the bottom left corner indicate main [1$\bar{1}$0] crystal directions of the gold lattice. (A) Parent STM image. (B) STM image in which the unit cells, as determined by the correlation method, are drawn in as red and green dots, which represent the two unique domains that are present (E and F).

reconstruction. Such a superposition of two lattices into a superstructure with an irregular unit cell that differs from each of the unit cells of the superimposed lattices can occur if these lattices are incommensurable. This is clearly the case for domain D, and the absence of a regular unit cell has been indicated in figure 5(B) by drawing in the widths of two distinctly different superstructure periods (5.5 and 6.2 nm, respectively).

The distribution of the unit cells shown in figure 5(B) and, in particular, the two-by-one organization of porphyrins within the unit cells in domains A, B and C are reminiscent of the previously observed lamellar organization of *n*-tetradecane on Au(111). In particular, the molecules of Mn1 in domains B and C would fit well on a typical *n*-tetradecane monolayer; the short lattice vector $\vec{a}$ would be along the direction of the *n*-tetradecane lamellae, and the height of the unit cell perpendicular to vector $\vec{a}$ (17.9 ± 0.5 Å) matches the observed lamellar width (16.4–17.4 Å) quite well. Although ill-determined, the domain boundaries between the domains A, B and C are directed approximately along the ⟨1$\bar{1}$0⟩-direction of the gold lattice, in a similar way as has been previously observed for the boundaries between the different *n*-tetradecane domains. Although the measurements in figure 5 yield no conclusive evidence, they strongly suggest that the ordering of the domains A, B and C of the monolayer of Mn1 is determined or at least strongly influenced by an *n*-tetradecane monolayer, which is either still hidden underneath the porphyrins, or has influenced the adsorption of the molecules of Mn1 but is no longer present. Whether such an *n*-tetradecane monolayer has had a similar influence on the porphyrin lattice in domain D is impossible to say based on these STM measurements,

as the superstructure caused by the reconstruction herringbone conceals any subtle effects this monolayer might have had. From the multitude of STM measurements that were performed on this system it appeared that the porphyrin ordering observed in domain D is the most commonly occurring morphology, often covering the entire surface (figure 6). The superstructure is most clearly identified in the image in figure 6(A) by the presence of porphyrin rows with an increased brightness, which is proposed to be caused by a superposition of the herringbone reconstruction of the Au(111) surface and the porphyrin lattice. This observation strongly indicates that there is an influence of this reconstruction on the formation of the monolayer of Mn1, and that the porphyrin ordering, which is templated by this reconstruction, is the thermodynamically most favorable one.

4. Conclusions

Using the liquid-cell STM, we have been able to study a clean and well-defined solid–liquid interface between *n*-tetradecane and an Au(111) surface on which the typical $23 \times \sqrt{3}$ surface reconstruction remained intact. At the interface, an ordered monolayer of *n*-tetradecane was present that does not influence the reconstruction in an appreciable way. This observation indicates that there is a low interaction between the metal surface and the *n*-tetradecane molecules, which is also apparent from the observed fact that the orientation of the *n*-tetradecane monolayer is not fixed with respect to the Au(111) crystal structure.

The growth of a monolayer of Mn1 at this solid–liquid interface can be templated by an initially present herringbone reconstruction of the Au(111) surface. The monolayer morphology that is templated by the reconstruction is the most frequently occurring and probably the thermodynamically most stable one, but there are also less frequently occurring morphologies that indicate a pronounced influence of an *n*-tetradecane monolayer at the surface. Current research is focused on investigating the influence of the morphology of the monolayer on the catalytic oxidation properties of the manganese porphyrins.

Acknowledgments

NanoNed (the Dutch nanotechnology initiative by the Ministry of Economic Affairs), the Council for the Chemical Sciences of the Netherlands Organization for Scientific Research (CW-NWO) and the Australian Research Council are acknowledged for financial support.

References

[1] Roeffaers M B J, Sels B F, Uji-i H, De Schryver F C, Jacobs P A, de Vos D E and Hofkens J 2006 *Nature* **439** 572
Roeffaers M B J, De Cremer G, Uji-i H, Muls B, Sels B F, Jacobs P A, De Schryver F C, De Vos D E and Hofkens J 2007 *Proc. Natl Acad. Sci. USA* **104** 12603

[2] Lu H P, Xu L and Xie X S 1998 *Science* **282** 1877
Velonia K *et al* 2005 *Angew. Chem., Int. Ed. Engl.* **44** 560
Flomenbom O *et al* 2005 *Proc. Natl Acad. Sci. USA* **102** 2368
Hatzakis N S *et al* 2006 *Chem. Commun.* 2012
Martínez Martínez V, De Cremer G, Roeffaers M B J, Sliwa M, Baruah M, De Vos D E, Hofkens J and Sels B F 2008 *J. Am. Chem. Soc.* **130** 13192

[3] Hla S-W, Bartels L, Meyer G and Rieder K-H 2000 *Phys. Rev. Lett.* **85** 2777
Hendriksen B L M and Frenken J W M 2002 *Phys. Rev. Lett.* **89** 046101
Weigelt S *et al* 2007 *Angew. Chem., Int. Ed. Engl.* **46** 9227
Grill L, Dyer M, Lafferentz L, Persson M, Peters M V and Hecht S 2007 *Nat. Nanotechnol.* **2** 687
Weigelt S *et al* 2007 *Angew. Chem., Int. Ed. Engl.* **46** 9227
Zwaneveld N A A, Pawlak R, Abel M, Catalin D, Gigmes D, Bertin D and Porte L 2008 *J. Am. Chem. Soc.* **130** 6678
Matena M, Riehm T, Stöhr M, Jung T A and Gade L H 2008 *Angew. Chem.* **120** 2448
Matena M, Riehm T, Stöhr M, Jung T A and Gade L H 2008 *Angew. Chem., Int. Ed. Engl.* **47** 2414
In't Veld M, Iavicoli P, Haq S, Amabilino D B and Raval R 2008 *Chem. Commun.* 1536
Treier M, Richardson N V and Fasel R 2008 *J. Am. Chem. Soc.* **130** 14054
[4] Hulsken B, Gerritsen J W and Speller S 2005 *Surf. Sci.* **580** 95
[5] Samorì P 2004 *J. Mater. Chem.* **14** 1353
Elemans J A A W and De Feyter S 2009 *Soft Matter* **5** 721
[6] Hulsken B, van Hameren R, Gerritsen J W, Khoury T, Thordarson P, Crossley M J, Rowan A E, Nolte R J M, Elemans J A A W and Speller S 2007 *Nat. Nanotechnol.* **2** 285
[7] Hulsken B, van Hameren R, Thordarson P, Gerritsen J W, Nolte R J M, Rowan A E, Crossley M J, Elemans J A A W and Speller S 2006 *Japan. J. Appl. Phys.* **45** 1953
[8] Gerritsen J W, Boon E J G, Janssens G and van Kempen H 1998 *Appl. Phys.* A **66** S79
[9] Soethout L L, Gerritsen J W, Groeneveld P P M C, Nelissen B J and van Kempen H 1988 *J. Microsc.* **152** 251
[10] Marchenko A and Lukyanets S 2002 *Phys. Rev.* B **65** 045414
[11] Bürgi L, Brune H and Kern K 2002 *Phys. Rev. Lett.* **89** 176801
[12] Xia T K, Ouyang J, Ribarsky M W and Landman U 1992 *Phys. Rev. Lett.* **69** 1967
[13] Cousty J and Marchenko A 2002 *Surf. Sci.* **520** 128